

Output control of dissipative nonlinear multimode amplifiers using spacetime symmetry mapping

Received: 6 April 2024

Accepted: 27 February 2025

Published online: 1 April 2025

 Check for updates

Chun-Wei Chen^{1,4}, Kabish Wisal^{2,4}, Mathias Fink³, A. Douglas Stone¹ & Hui Cao¹✉

In many linear and nonlinear systems, time-reversal symmetry makes it possible to control the output waves by appropriately shaping the input waves. However, time-reversal symmetry is broken in systems with energy dissipation, necessitating a different approach for relating the input and output fields. We theoretically consider a saturated multimode fibre amplifier in which light generates a heat flow and suffers thermo-optical nonlinearity, thus breaking time-reversal symmetry. We identify a spacetime symmetry that maps the target output back to an input field. This spacetime symmetry mapping applies phase conjugation, gain and absorption substitution but not time reversal, and it holds in a steady state and for slowly varying inputs. Our approach enables coherent wavefront control of nonlinear dissipative systems.

Time-reversal symmetry and reciprocity have been widely explored with various types of waves, including electromagnetic, acoustic and water waves^{1–3}. The invention of time-reversal mirrors^{4–7} and optical phase conjugators^{8–10} has enabled a wide range of applications, such as aberration correction^{11–13}, dispersion compensation¹⁴, and spatial and temporal refocusing^{15–22}, which have practical impact in imaging, communications, spectroscopy and sensing^{23–29}. In general, time-reversal symmetry holds not only for linear but also nonlinear processes, as long as the waves are not coupled to a bath by an irreversible process^{30–32}. For example, the Kerr-effect-induced self-phase modulation and multi-wave mixing can be reversed to undo a pulse distortion³³, remove the spectral broadening³⁴ and even reconstruct rogue waves^{35,36}. A common application of time-reversal symmetry is to create a wavefront that can autonomously refocus itself after scattering by time-reversing the fields generated by a point source in the desired focal position. Once identified, the refocusing wavefront can be synthesized experimentally and fed back into the same system to achieve focusing. A dissipative process, such as linear amplification, does break time-reversal invariance, but the input wavefront can still be found by mapping to a different system with loss replacing gain, as has been illustrated, for example, in the study of coherent

perfect absorption (time-reversed lasing)^{37,38}. In this case, the phase conjugation and replacing the gain with loss in the steady-state wave equation identifies a wavefront that will be completely trapped and absorbed by the time-reversed counterpart. Such mappings, which interchange gain and loss to find the solution to an inverse problem, exist even in the presence of nonlinearity and chaos^{39,40}.

The high-power multimode optical fibre amplifier studied here is unlike the nonlinear dissipative systems previously studied; it is characterized by heat diffusion, thermo-optical nonlinearity and gain saturation^{41–43}. As the light is amplified, heat is necessarily generated because of the non-radiative transitions in the pumping cycle, and this heat diffuses irreversibly out of the fibre to the surrounding reservoir. The first derivative of the temperature with respect to time in the thermal diffusion equation reflects this irreversibility and, thus, breaks time-reversal symmetry. Even if we map this system to a conjugate system with the optical gain replaced by an equal amount of absorption, heat will still be generated in the fibre and flow to the reservoir. Thus, the two systems are not time-reversed counterparts in general, and reversing the output signal from a multimode fibre (MMF) amplifier and launching it to the complementary MMF with absorption will not reproduce the original input to the amplifier. Moreover,

¹Department of Applied Physics, Yale University, New Haven, CT, USA. ²Department of Physics, Yale University, New Haven, CT, USA. ³Institut Langevin, ESPCI Paris, CNRS, PSL University, Paris, France. ⁴These authors contributed equally: Chun-Wei Chen, Kabish Wisal. ✉e-mail: hui.cao@yale.edu

the non-uniform heating of the fibre, arising from the spatially varying intensity distribution of the multimode interference, causes a non-uniform index change because of the thermo-optical nonlinearity and scatters light between fibre modes. As the power increases in the fibre, dynamic mode coupling will destabilize the MMF amplifier and the quality of the output beam degrades due to an effect termed the transverse mode instability (TMI)⁴⁴.

Recent studies reveal that increasing the number of excited modes in a MMF will suppress TMI, enabling further power scaling of fibre amplifiers^{45,46}. However, even in the absence of TMI, multimode interference will generate speckled fields at the output, which is undesirable for practical applications. Unlike in a linear MMF without gain, simply phase-conjugating a desired output field profile and sending it back into the fibre amplifier will not generate the required input wavefront. Recently, it was shown experimentally that shaping the wavefront of a coherent seed to a MMF amplifier can focus the output light^{47,48}. However, it was not known whether it is possible to generate any desired output beam profile of a MMF amplifier by shaping the input wavefront.

We present a spacetime symmetry mapping showing that, indeed, there is an input wavefront with a specific power that can generate an arbitrary output beam profile at any chosen power, as long as the fibre amplifier operates below the TMI threshold. Our mapping is a generalization of the more familiar gain–loss mapping between an amplifier and its absorbing counterpart. With a monochromatic time-invariant seed, the amplifier reaches a steady state and produces a static output field. In the complementary fibre with absorption, the amplifier output is phase-conjugated and sent back to the distal end. As we will show, the power growth in the nonlinear amplifier with saturated gain is exactly reversed in the absorbing fibre with an identical saturation intensity for absorption. Assuming that the same amount of heat is generated in the fibre and flows into the thermal bath, the phase-conjugated field undergoes nonlinear thermo-optical scattering, which reverses the effect of the nonlinear-mode coupling in the amplifier. Therefore, the steady-state transmitted field at the proximal end of the absorbing MMF is identical to the phase-conjugated input of the amplifying fibre, proving that any target amplifier output can be generated by wavefront-shaping a coherent monochromatic seed.

The spacetime symmetry mapping also holds for a dynamic amplifier with time-varying input and output fields. The target dynamic output from the amplifier is phase-conjugated but not time-reversed before it is sent to the absorbing fibre. The transmitted field provides the phase-conjugated input to the amplifier, and the resulting output has a negligible difference from the desired one. This mapping relies on the thermal response time (milliseconds) being much longer than the optical response time (nanoseconds) in a typical fibre amplifier and further requires that the input and output field envelopes are slowly varying compared to the optical response time, such that dynamic changes of temperature and refractive index are negligible during the time of flight for light through the fibre.

Our spacetime symmetry mapping proves that there exists an input wavefront that can produce any output beam profile in a nonlinear MMF amplifier below the instability threshold. This generalization of symmetry-based mappings beyond time-reversal to describe nonlinear dissipative systems not only advances our physical understanding of complex wave phenomena but also broadens the range of applications for coherent wave control.

Thermo-optical nonlinearity

We now present the analytic and numerical results that validate this argument. Consider coherent, narrowband light of frequency ω_0 launched into a MMF amplifier of length L . The electric field can be decomposed by the fibre modes as:

$$\psi(r_{\perp}, z, t) = \sum_m \phi_m(r_{\perp}) A_m(z, t) e^{i\beta_m z - i\omega_0 t}. \quad (1)$$

The fibre is parallel to the z axis, extending from $z = 0$ to L , and r_{\perp} can denote any number of transverse coordinates (perpendicular to the fibre axis). The m th guided mode in the passive fibre has the transverse field profile $\phi_m(r_{\perp})$ and (axial) propagation constant β_m . $A_m(z, t)$ is the complex amplitude of the field in the m th mode at position z and time t .

In the slowly varying approximation for $A_m(z, t)$, the scalar paraxial optical wave equation gives

$$\frac{\partial A_m(z, t)}{\partial z} + \frac{1}{v_m} \frac{\partial A_m(z, t)}{\partial t} = \left(i\beta_m + \frac{g_m}{2} \right) A_m(z, t) + i \sum_j A_j(z, t) \left[\gamma_{m,j} + k_0 \eta e^{i(\beta_j - \beta_m)z} \int \phi_j(r_{\perp}) \Delta T(r_{\perp}, z, t) \phi_m(r_{\perp}) dr_{\perp} \right], \quad (2)$$

where v_m is the velocity of the m th mode, g_m denotes the mode-dependent gain, $\gamma_{m,j}$ represents the linear-mode coupling coefficient and k_0 is the vacuum wavenumber. The frequency of the pump light ω_p is higher than that of the emission ω_0 , causing quantum-defect heating $Q(r_{\perp}, z, t) \propto (\omega_p/\omega_0 - 1)I(r_{\perp}, z, t)$ that depends on the local intensity $I(r_{\perp}, z, t) = |\psi(r_{\perp}, z, t)|^2$. Multimode interference results in a highly speckled intensity distribution throughout the fibre, and non-uniform heating causes local variations of the temperature $\Delta T(r_{\perp}, z, t)$. Owing to the thermo-optical nonlinearity, the temperature change induces a refractive-index variation through the thermo-optic coefficient $\eta = 2n(dn/dT)$. The spatial and temporal change of the index $\Delta n(r_{\perp}, z, t)$ introduces nonlinear coupling between fibre modes, as represented by the last term of equation (2).

The heat diffusion equation is

$$\rho C \frac{\partial \Delta T(r_{\perp}, z, t)}{\partial t} - \kappa \left(\frac{\partial^2}{\partial r_{\perp}^2} + \frac{\partial^2}{\partial z^2} \right) \Delta T(r_{\perp}, z, t) = Q(r_{\perp}, z, t) = |g(r_{\perp}, z, t)| q_D I(r_{\perp}, z, t), \quad (3)$$

where ρ is the mass density, C is the specific heat capacity, κ is the thermal conductivity, Q is the rate of heat generation per unit volume, $g(r_{\perp}, z, t)$ is the local gain coefficient and $q_D = \omega_p/\omega_0 - 1$ represents the quantum defect.

The thermo-optical nonlinearity involves processes on different timescales, as detailed in Supplementary Information Section I. The thermal response time, determined by quantum-defect heating and thermal diffusion, is of the order of milliseconds in a Yb-doped MMF amplifier. Thus, the temperature distribution can be considered static during the transit time (nanoseconds) of light in a fibre of typical length ~ 1 – 10 m. For a given temperature distribution, the optical response time, that is, the time it takes for the optical field distribution throughout the fibre to reach a steady state, is of the order of nanoseconds.

Steady state

First, we consider the case in which the fibre amplifier reaches a steady state when excited with a time-invariant seed signal. In the optical and heat equations, $\partial/\partial t = 0$, and equations (2) and (3) reduce to:

$$\frac{\partial A_m(z)}{\partial z} = \left(i\beta_m + \frac{g_m}{2} \right) A_m(z) + i \sum_j A_j(z) \left[\gamma_{m,j} \right. \quad (4)$$

$$\left. + k_0 \eta e^{i(\beta_j - \beta_m)z} \int \phi_j(r_{\perp}) \Delta T(r_{\perp}, z) \phi_m(r_{\perp}) dr_{\perp} \right]$$

and

$$-\kappa \left(\frac{\partial^2}{\partial r_{\perp}^2} + \frac{\partial^2}{\partial z^2} \right) \Delta T(r_{\perp}, z) = |g(r_{\perp}, z)| q_D I(r_{\perp}, z), \quad (5)$$

respectively.

If $\{A_m\}$ satisfies equations (4) and (5), then $\{A_m^*\}$ satisfies the complex conjugate of equations (4) and (5), which corresponds to switching the gain g_m to absorption $-g_m$ and the forward propagation in z to backward propagation $-z$. All coefficients and constants including q_b are kept the same. These equations govern the time-reversed counterpart of the steady-state MMF amplifier. Although the field is complex-conjugated, the intensity distribution is unchanged. Although the atomic transitions in the absorbing fibre will not be reversed, we simply assume that the same amount of heat will be generated by absorption in the fibre. Then the temperature distribution will be unchanged, as the thermal boundary conditions are identical. As the equations for the time-reversed counterpart of the steady-state MMF amplifier are invariant, ‘sending back’ the conjugated output will produce the original input field, conjugated.

To confirm this argument for the steady-state condition, we performed numerical simulations in the time domain. We considered a waveguide with a one-dimensional cross section and core width $w = 40 \mu\text{m}$, cladding width $W = 400 \mu\text{m}$, refractive index $n = 1.5$ and length $L = 1 \text{m}$. For simplicity, we assumed perfect reflection of light from the core–cladding interface and neglected linear-mode coupling, $\gamma_{m,j} = 0$. We also assumed that the optical gain g_m is linear (the gain saturation is considered later) and identical for all modes. The outer boundaries of the cladding are perfectly thermally conducting. Further details of the simulation and relevant timescales are given in Supplementary Information Sections I, II and III.

Figure 1 shows the numerical result for one representative example. A coherent, monochromatic seed was launched into the waveguide at $z = 0$ and amplified from 30 W at $z = 0$ to 270 W at $z = L$. The steady-state output field profile was very different from the input, due to modal dispersion and thermo-optical mode coupling. The output field pattern was phase-conjugated and launched into a waveguide with absorption ($g_m \rightarrow -g_m$) from the distal end. The power was reduced back to 30 W at the proximal end, and the steady-state output field pattern of the absorptive waveguide was, indeed, the same as the original input to the amplifier (with conjugated phase) to high accuracy. The temperature distribution was identical in the two cases, validating our argument for the steady-state case.

Note that random linear-mode coupling, which was neglected in the above simulation, does not affect the validity of our spacetime symmetry mapping, as long as it remains constant during the transit time of light through the fibre. This is confirmed in the numerical results of strong linear-mode coupling in Supplementary Information Section IV.

Gain saturation

Next, we include another saturating nonlinearity in the multimode amplifier. In the steady state, $g_m = g_m^{(0)} / [1 + I(r_{\perp}, z) / I_{\text{sat}}]$, where $g_m^{(0)}$ denotes the small-signal gain for the m th mode of the fibre and I_{sat} is the saturation intensity of a MMF amplifier. The presence of gain saturation in real amplifiers has important physical effects. As the degree of saturation depends on the spatially varying intensity, the gain distribution becomes spatially inhomogeneous in both the transverse and longitudinal directions. Hence, the nonlinear gain becomes mode-dependent, which modifies the growth rate of individual modes and their interference throughout the fibre. The resulting intensity changes alter the heat generation and temperature distribution. Consequently, the thermo-optical coupling between fibre modes is substantially modified by gain saturation, and the output field pattern changes dramatically.

However, there is still the time-reversed counterpart of a steady-state MMF amplifier. The saturated gain is replaced by saturated absorption. In the time-reversed counterpart, the optical absorption $-g_m$ is saturated by the same amount as the optical gain, because the intensity distribution is unchanged and I_{sat} is identical. We verified this explicitly with time-domain numerical simulations, and the results are shown in Fig. 2 (details in the caption). We used

the time-reversed counterpart to obtain an input wavefront that focuses to a diffraction-limited spot after propagating through the waveguide amplifier with gain saturation and thermo-optical nonlinearity. This opens up important practical applications for obtaining high-quality beams at the output of MMF amplifiers, which could provide a much higher stable output power than single-mode fibre amplifiers⁴⁵. Although the MMF amplifiers in our numerical simulations have a one-dimensional cross section to reduce the computational load, our theoretical analyses based on spacetime symmetry mapping are valid for any number of dimensions and for any transverse geometry (Supplementary Information Section II).

Time-varying input

In the previous examples, the multimode amplifier reached a steady state with a time-invariant seed and the time derivative of the envelope dropped out. We now consider a dynamic state of the amplifier, in which both the amplitude and phase of the input envelope vary on a timescale of 0.1–1 ms, like that of the temperature changes. Figure 3a shows an example of the output generated by the amplifier for such a seed. For computational simplicity, in this time-varying case, we consider only two modes in a 0.1-m-long fibre and neglect gain saturation. Analysing equations (2) and (3), we see that phase-conjugating the output field and sending it back into the absorptive waveguide without reversing the envelope in time corresponds to the mapping $z \rightarrow -z, t \rightarrow t, g_m \rightarrow -g_m, A_m(z, t) \rightarrow A_m^*(-z, t)$ and $\Delta T(r_{\perp}, z, t) \rightarrow \Delta T(r_{\perp}, -z, t)$. The heat equation (3) remains invariant, but the optical equation (2) is not due to the $(1/v_m)\partial A_m(z, t)/\partial t$ term. However, this term is much smaller than $\partial A_m(z, t)/\partial z$ and can be neglected, as the optical pulse envelope evolves temporally on the thermal response time, which is much longer than the nonlinear optical response time in the fibre. Ignoring $(1/v_m)\partial A_m(z, t)/\partial t$ means that the optical equation also remains invariant under our proposed mapping. Hence, we propagated backwards in space the conjugated output of Fig. 3a in Fig. 3b without reversing the direction of time, and indeed, we found that this generated a transmitted field almost identical to the phase-conjugated input to the waveguide amplifier. Note that the naive time-reversal operation with an extra mapping $t \rightarrow -t$ satisfies the equation for light propagation, equation (2), but not that for heat diffusion, equation (3). Hence, this mapping does not reproduce the conjugated input field, as confirmed numerically in Fig. 3c. A phase-conjugated, time-reversed, output field propagated backward in the waveguide with absorption created a transmitted field completely different from the original input to the waveguide amplifier (Fig. 3c). See Supplementary Information Sections VI and VII for more simulation details and a discussion.

Discussion

In summary, we have identified a spacetime symmetry mapping that proves the existence of an input field profile at a specific power that generates a desired output field profile at a chosen power for a MMF amplifier with both thermo-optical and saturating nonlinearities. This mapping is valid for both steady-state inputs and slowly varying pulses, but it will fail when the power is high enough to cause a dynamical instability, such as TMI (for a further discussion, see Supplementary Information Section VIII). This limitation is like that in other nonlinear systems in the regime of dynamical chaos or instability, where even if time-reversal symmetry exists, noise and sensitivity to small perturbations make it impractical to exploit.

Our results extend our understanding of the possibilities of wave control after nonlinear propagation in dissipative media. In particular, this work implies the possibility of generating any output beam profile for a high-power amplifier, including a diffraction-limited focal spot that can be collimated subsequently to the far field. Given the concerns regarding the output beam quality for high-power fibre amplifiers^{41–43}, our results pave the way for employing MMF amplifiers in high-power applications, thus leveraging their advantages over the single-mode

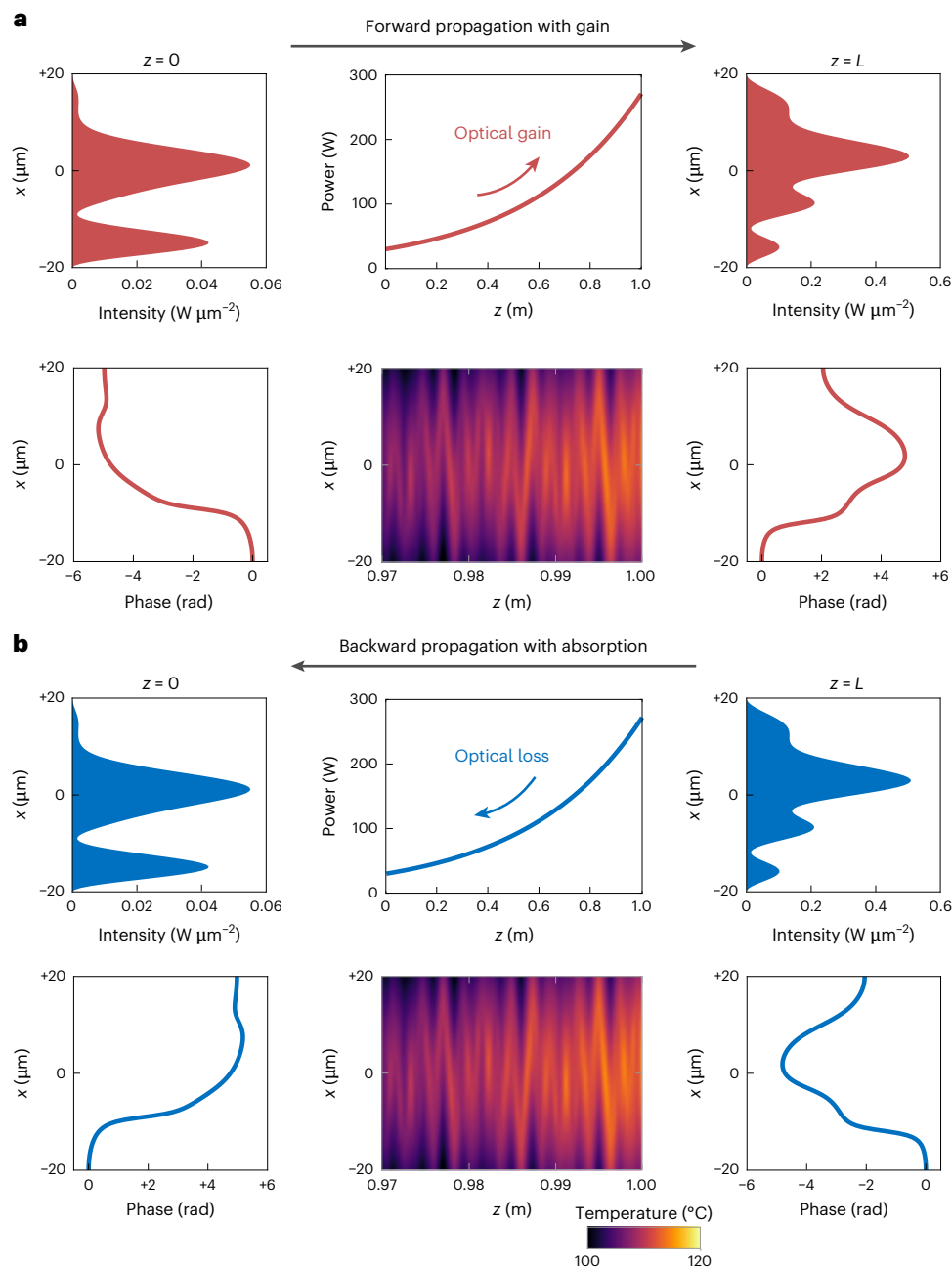


Fig. 1 | Steady-state time-reversal of a multimode amplifier with thermo-optical nonlinearity and linear gain. **a**, A 30-W monochromatic input at a wavelength of 1,064 nm with a time-invariant wavefront excites five modes in a 1-m-long waveguide amplifier with a one-dimensional cross section (along x). With a linear, mode-independent, gain coefficient $g = 2.2 \text{ m}^{-1}$, the amplified output reaches 270 W. The steady-state temperature profile reveals non-uniform heating caused by an inhomogeneous intensity distribution throughout the waveguide. Even without linear-mode coupling, thermo-optical coupling and

modal dispersion make the output wavefront very different from the input.

b, When the output of the amplifier is phase-conjugated and launched backward at the distal end of a complementary waveguide with absorption, the wavefront distortion is removed, and the input to the amplifier is recovered (with a conjugated phase). The same amount of heat is generated, and the temperature profile is identical to that in **a**. In both cases, the temperature at the outer boundary of the waveguide cladding was set to 20 °C.

counterparts, for example, high-power thresholds for TMI^{45,46} and stimulated Brillouin scattering^{49,50}. Note that such wavefront-shaping schemes work well only for narrowband amplifiers; specifically, when the spectral bandwidth of an input signal is less than the spectral correlation width of the output field pattern.

Although the spacetime symmetry mapping proves the existence of an input wavefront to produce any output beam profile for a nonlinear MMF amplifier, the physical implementation of such a mapping is difficult. Experimentally, the input wavefront could be adjusted to minimize the difference between the output pattern and the target

one. Such feedback optimization has been used to focus the output beam of a MMF amplifier with weak nonlinearity to a spot at a chosen location^{47,48}. Alternatively, an artificial neural network that maps the MMF amplifier output to its input may be trained with experimental data to predict the input wavefront for any desired output pattern. However, these methods do not guarantee a priori that the required input exists in the presence of strong nonlinearities. Hence, our theoretical proof based on the spacetime symmetry mapping lays a solid foundation for experimental wavefront-shaping methods in nonlinear dissipative systems.

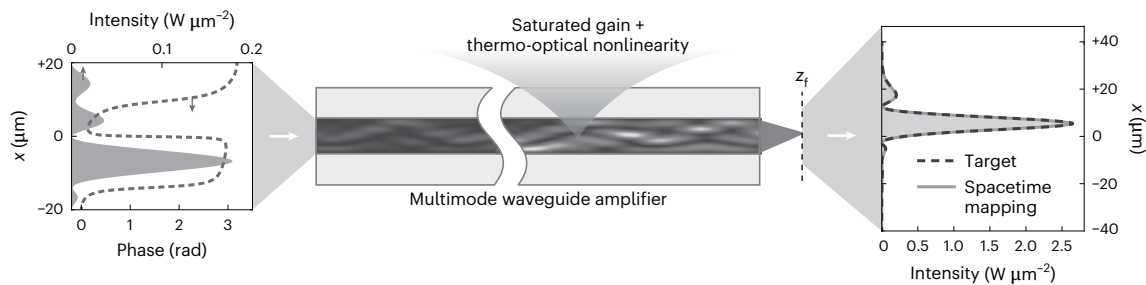


Fig. 2 | Focusing through a nonlinear multimode amplifier with gain saturation. The input wavefront of a monochromatic seed (at 60 W) to a five-mode waveguide amplifier is shaped with thermo-optical nonlinearity and gain saturation to focus the amplified output (at 750 W) to a designated location ($z_f = 116 \mu\text{m}$ beyond the end facet and $5 \mu\text{m}$ from the waveguide axis). The small-signal gain coefficient is 7.0 m^{-1} , and the saturation intensity is

$0.0625 \text{ W } \mu\text{m}^{-2}$. The input wavefront is obtained by sending the focused output through a complementary waveguide with saturable absorption and then phase-conjugating the transmitted field profile, which is the spacetime-mapping approach. The focused output from the amplifier exhibits a diffraction-limited spot of width $10 \mu\text{m}$, and small side lobes can be effectively suppressed by increasing the number of waveguide modes that contribute to output focusing.

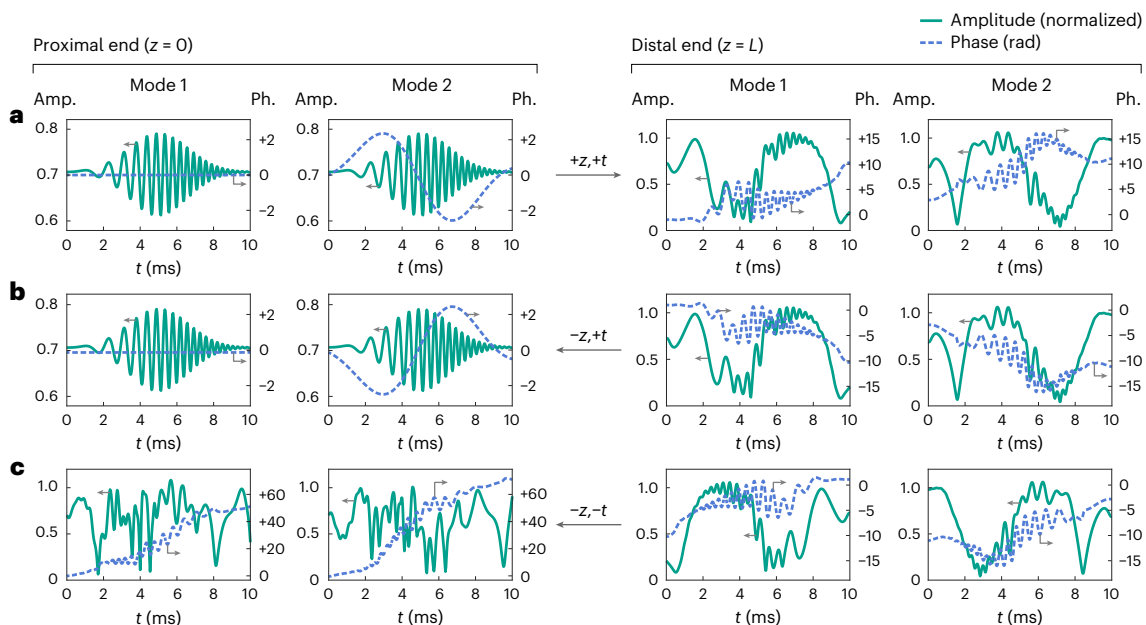


Fig. 3 | Spacetime symmetry mapping of a dynamic nonlinear amplifier. **a–c.** Time traces of the field amplitude and phase of a two-mode waveguide amplifier at the proximal and distal ends. **a.** A time-varying field with a peak power of 237 W was launched into a 0.1-m-long waveguide amplifier with two modes equally excited at $z = 0$. The amplitudes of the input fields of both modes have the same Gaussian envelope and are temporally chirped at -2.1 kHz . Although mode 1 has a time-invariant phase, mode 2 has a phase modulation at -0.1 kHz . The amplified field reached a peak power of 300 W at $z = L$. Heat-induced dynamic

mode coupling in the waveguide caused a spatio-temporal distortion of the output field. In each diagram, the time-varying mode amplitudes were normalized by the time-averaged total power. **b.** Phase conjugation without time reversal of the amplifier output was sent to the absorbing waveguide. The transmitted field was almost identical to the phase-conjugated input to the amplifier. **c.** Phase-conjugated, time-reversed output field of the amplifier was launched into a complementary waveguide with absorption at $z = L$. The transmitted field at $z = 0$ is wholly different from the amplifier input. Amp., amplitude; Ph., phase.

More broadly, the spacetime symmetry mapping method is adaptable to any type of nonlinearity, provided that the nonlinearity does not induce instability (see Supplementary Information Section V for details of the optical Kerr nonlinearity). Beyond optical waves, our scheme is general and applicable to other types of waves. It paves the way for the non-equilibrium control of nonlinear dissipative processes in complex open systems.

Online content

Any methods, additional references, Nature Portfolio reporting summaries, source data, extended data, supplementary information, acknowledgements, peer review information; details of author contributions and competing interests; and statements of data and code availability are available at <https://doi.org/10.1038/s41567-025-02853-5>.

References

1. Fink, M. Time reversal in acoustics. *Contemp. Phys.* **37**, 95–109 (1996).
2. Potton, R. J. Reciprocity in optics. *Rep. Prog. Phys.* **67**, 717 (2004).
3. Pradka, A. et al. Time reversal of water waves. *Phys. Rev. Lett.* **109**, 064501 (2012).
4. Fink, M. Time-reversal mirrors. *J. Phys. D* **26**, 1333 (1993).
5. Fink, M. & Prada, C. Acoustic time-reversal mirrors. *Inverse Probl.* <https://doi.org/10.1088/0266-5611/17/1/201> (2001).
6. Kuperman, W. et al. Phase conjugation in the ocean: experimental demonstration of an acoustic time-reversal mirror. *J. Acoust. Soc. Am.* **103**, 25–40 (1998).
7. Mounaix, M. et al. Time reversed optical waves by arbitrary vector spatiotemporal field generation. *Nat. Commun.* **11**, 5813 (2020).

8. Zel'Dovich, B. Y., Popovichev, V., Ragul'Skii, V. & Faizullov, F. in *Landmark Papers on Photorefractive Nonlinear Optics* (eds Yeh, P. & Gu, C.) 303–306 (World Scientific, 1995).
9. Bloom, D. M. & Bjorklund, G. C. Conjugate wave-front generation and image reconstruction by four-wave mixing. *Appl. Phys. Lett.* **31**, 592–594 (1977).
10. Yariv, A. & Pepper, D. M. Amplified reflection, phase conjugation, and oscillation in degenerate four-wave mixing. *Opt. Lett.* **1**, 16–18 (1977).
11. Nosach, O. Y., Popovichev, V. I., Ragul'Skii, V. & Faizullov, F. Cancellation of phase distortions in an amplifying medium with a 'Brillouin mirror'. *ZHETF Pis ma Redaktsiiu* **16**, 617 (1972).
12. Wang, V. & Giuliano, C. R. Correction of phase aberrations via stimulated Brillouin scattering. *Opt. Lett.* **2**, 4–6 (1978).
13. Agarwal, G., Friberg, A. T. & Wolf, E. Scattering theory of distortion correction by phase conjugation. *J. Opt. Soc. Am.* **73**, 529–538 (1983).
14. Yariv, A., Fekete, D. & Pepper, D. M. Compensation for channel dispersion by nonlinear optical phase conjugation. *Opt. Lett.* **4**, 52–54 (1979).
15. Lerosey, G., De Rosny, J., Tourin, A. & Fink, M. Focusing beyond the diffraction limit with far-field time reversal. *Science* **315**, 1120–1122 (2007).
16. Yaqoob, Z., Psaltis, D., Feld, M. S. & Yang, C. Optical phase conjugation for turbidity suppression in biological samples. *Nat. Photonics* **2**, 110–115 (2008).
17. Papadopoulos, I. N., Farahi, S., Moser, C. & Psaltis, D. Focusing and scanning light through a multimode optical fiber using digital phase conjugation. *Opt. Express* **20**, 10583–10590 (2012).
18. Dezfooliyani, A. & Weiner, A. M. Spatiotemporal focusing of phase compensation and time reversal in ultrawideband systems with limited rate feedback. *IEEE Trans. Veh. Technol.* **65**, 1998–2006 (2015).
19. Feldkhun, D., Tzang, O., Wagner, K. H. & Piestun, R. Focusing and scanning through scattering media in microseconds. *Optica* **6**, 72–75 (2019).
20. Baek, Y., de Aguiar, H. B. & Gigan, S. Phase conjugation with spatially incoherent light in complex media. *Nat. Photonics* **17**, 1114–1119 (2023).
21. Cheng, Z., Li, C., Khadria, A., Zhang, Y. & Wang, L. V. High-gain and high-speed wavefront shaping through scattering media. *Nat. Photonics* **17**, 299–305 (2023).
22. Bureau, F. et al. Three-dimensional ultrasound matrix imaging. *Nat. Commun.* **14**, 6793 (2023).
23. Yariv, A. Phase conjugate optics and real-time holography. *IEEE J. Quantum Electron.* **14**, 650–660 (1978).
24. Pepper, D. M. Nonlinear optical phase conjugation. *Opt. Eng.* **21**, 212156 (1982).
25. Rouseff, D. et al. Underwater acoustic communication by passive-phase conjugation: theory and experimental results. *IEEE J. Ocean. Eng.* **26**, 821–831 (2001).
26. Popoff, S., Lerosey, G., Fink, M., Boccarda, A. C. & Gigan, S. Image transmission through an opaque material. *Nat. Commun.* **1**, 81 (2010).
27. Fisher, R. A. (ed.) *Optical Phase Conjugation* (Academic, 2012).
28. Mosk, A. P., Lagendijk, A., Lerosey, G. & Fink, M. Controlling waves in space and time for imaging and focusing in complex media. *Nat. Photonics* **6**, 283–292 (2012).
29. Alexandropoulos, G. C. et al. Time reversal for 6G spatiotemporal focusing: recent experiments, opportunities, and challenges. *IEEE Veh. Technol. Mag.* **17**, 74–82 (2022).
30. Tanter, M., Thomas, J.-L., Coulouvrat, F. & Fink, M. Breaking of time reversal invariance in nonlinear acoustics. *Phys. Rev. E* **64**, 016602 (2001).
31. Ducrozet, G., Fink, M. & Chabchoub, A. Time-reversal of nonlinear waves: applicability and limitations. *Phys. Rev. Fluids* **1**, 054302 (2016).
32. Fernandes, D. E. & Silveirinha, M. G. Role of time-reversal symmetry in the dynamical response of one-way nonlinear devices. *Phys. Rev. Appl.* **18**, 024002 (2022).
33. Pepper, D. M. & Yariv, A. Compensation for phase distortions in nonlinear media by phase conjugation. *Opt. Lett.* **5**, 59–60 (1980).
34. Fisher, R. A., Suydam, B. & Yevick, D. Optical phase conjugation for time-domain undoing of dispersive self-phase-modulation effects. *Opt. Lett.* **8**, 611–613 (1983).
35. Chabchoub, A. & Fink, M. Time-reversal generation of rogue waves. *Phys. Rev. Lett.* **112**, 124101 (2014).
36. Ducrozet, G., Bonnefoy, F., Mori, N., Fink, M. & Chabchoub, A. Experimental reconstruction of extreme sea waves by time reversal principle. *J. Fluid Mech.* **884**, A20 (2020).
37. Chong, Y., Ge, L., Cao, H. & Stone, A. D. Coherent perfect absorbers: time-reversed lasers. *Phys. Rev. Lett.* **105**, 053901 (2010).
38. Pichler, K. et al. Random anti-lasing through coherent perfect absorption in a disordered medium. *Nature* **567**, 351–355 (2019).
39. Longhi, S. Time-reversed optical parametric oscillation. *Phys. Rev. Lett.* **107**, 033901 (2011).
40. Suwunnarat, S. et al. Non-linear coherent perfect absorption in the proximity of exceptional points. *Commun. Phys.* **5**, 5 (2022).
41. Cheng, M.-Y. et al. High-energy and high-peak-power nanosecond pulse generation with beam quality control in 200- μm core highly multimode yb-doped fiber amplifiers. *Opt. Lett.* **30**, 358–360 (2005).
42. Jauregui, C., Limpert, J. & Tünnermann, A. High-power fibre lasers. *Nat. Photonics* **7**, 861–867 (2013).
43. Zervas, M. N. & Codemard, C. A. High power fiber lasers: a review. *IEEE J. Sel. Top. Quantum Electron.* **20**, 219–241 (2014).
44. Jauregui, C., Stihler, C. & Limpert, J. Transverse mode instability. *Adv. Opt. Photonics* **12**, 429–484 (2020).
45. Chen, C.-W., Wisal, K., Eliezer, Y., Stone, A. D. & Cao, H. Suppressing transverse mode instability through multimode excitation in a fiber amplifier. *Proc. Natl Acad. Sci. USA* **120**, e2217735120 (2023).
46. Wisal, K., Chen, C.-W., Cao, H. & Stone, A. D. Theory of transverse mode instability in fiber amplifiers with multimode excitations. *APL Photonics* **9**, 066114 (2024).
47. Florentin, R. et al. Shaping the light amplified in a multimode fiber. *Light Sci. Appl.* **6**, e16208 (2017).
48. Florentin, R., Kermene, V., Desfarges-Berthelemot, A. & Barthelemy, A. Shaping of amplified beam from a highly multimode Yb-doped fiber using transmission matrix. *Opt. Express* **27**, 32638–32648 (2019).
49. Chen, C.-W. et al. Mitigating stimulated Brillouin scattering in multimode fibers with focused output via wavefront shaping. *Nat. Commun.* **14**, 7343 (2023).
50. Wisal, K., Warren-Smith, S. C., Chen, C.-W., Cao, H. & Stone, A. D. Theory of stimulated Brillouin scattering in fibers for highly multimode excitations. *Phys. Rev. X* **14**, 031053 (2024).
51. Chen, C.-W. et al. Dataset for 'Output control of dissipative nonlinear multimode amplifiers via spacetime symmetry mapping'. *Zenodo* <https://doi.org/10.5281/zenodo.14190653> (2024).

Publisher's note Springer Nature remains neutral with regard to jurisdictional claims in published maps and institutional affiliations.

Springer Nature or its licensor (e.g. a society or other partner) holds exclusive rights to this article under a publishing agreement with

the author(s) or other rightsholder(s); author self-archiving of the accepted manuscript version of this article is solely governed by the terms of such publishing agreement and applicable law.

© The Author(s), under exclusive licence to Springer Nature Limited 2025

Data availability

The data are available via Zenodo at <https://doi.org/10.5281/zenodo.14190653> (ref. 51).

Code availability

The codes are available at <https://github.com/joe851642001/MWAT>.

Acknowledgements

We thank Y. Eliezer for assisting in establishing the time-domain simulation code. We also thank A. Yamilov, O. D. Miller and S. Fan for fruitful discussions. This work is supported by the Air Force Office of Scientific Research (Grant No. FA9550-24-1-0182 to H.C. and A.D.S.) and by the Simons Foundation (A.D.S. and M.F.). We acknowledge the computational resources provided by the Yale High Performance Computing Cluster.

Author contributions

H.C. proposed the idea and initiated this project. C.-W.C. performed the numerical simulations under the supervision of H.C. K.W. performed the theoretical analysis under the supervision of A.D.S.

M.F. provided key insights that shaped the scope of this study. C.-W.C., K.W., A.D.S. and H.C. wrote the paper with input from M.F.

Competing interests

The authors declare no competing interests.

Additional information

Supplementary information The online version contains supplementary material available at <https://doi.org/10.1038/s41567-025-02853-5>.

Correspondence and requests for materials should be addressed to Hui Cao.

Peer review information *Nature Physics* thanks Mario Ferraro and the other, anonymous, reviewer(s) for their contribution to the peer review of this work.

Reprints and permissions information is available at www.nature.com/reprints.